Demonstration of lateral resolution enhancement by focusing amplitude modulated radially polarized light in a confocal imaging system

Meng, Peiwen; Pham, Hong Liên; Pereira, Silvania F.; Urbach, H. Paul

DOI
10.1088/2040-8986/ab7aeb

Publication date
2020

Document Version
Final published version

Published in
Journal of Optics (United Kingdom)

Demonstration of lateral resolution enhancement by focusing amplitude modulated radially polarized light in a confocal imaging system

OPEN ACCESS
IOP Publishing
Journal of Optics
J. Opt. 22 (2020) 045605 (5pp)
https://doi.org/10.1088/2040-8986/ab7aeb

Demonstration of lateral resolution enhancement by focusing amplitude modulated radially polarized light in a confocal imaging system

Peiwen Meng[1], Hong-Liên Pham[2], Silvania F Pereira[1] and H Paul Urbach[1]

[1] Optics Research Group, Department of Imaging Physics, Delft University of Technology, Lorentzweg 1, 2628CJ Delft, The Netherlands
[2] Institut d'Optique Graduate School, Elève 2A de l'Institut d'Optique Graduate School, Bordeaux, France

E-mail: P.Meng@tudelft.nl

Received 29 November 2019, revised 6 February 2020
Accepted for publication 27 February 2020
Published 16 March 2020

Abstract

Lateral resolution enhancement is demonstrated in a confocal imaging system with amplitude-modulated radially polarized (RP) light at the wavelength $\lambda = 632$ nm. Annular pupil fields and optimized amplitude distribution functions can be realized with a spatial light modulator. By comparing images obtained with full and amplitude modulated apertures of RP illuminations using a high numerical aperture (NA = 0.9), spatial resolution of $d = 0.358\lambda$ has been achieved experimentally. This result agrees very well with theoretical simulation results and will be helpful in improving performance of the non-fluorescent imaging systems.

Keywords: resolution, confocal imaging, polarization

(Some figures may appear in colour only in the online journal)

Radially polarized (RP) beams have attracted increasing interest due to their unique focusing properties. In the previous work, it has been shown that a RP beam focused by a high numerical aperture (NA) objective can generate a sharp focal spot because of its strong longitudinal component near focus [1, 2], which has potential in practical applications, such as optical tweezers and manipulation [3, 4], optical data storage [5], accelerators [6] and super-resolution microscopy [7]. However, one limitation is that although the longitudinal component dominates in three components of the focal field, the transverse component still exists and has a donut shape. The transverse component affects the optical process, especially the imaging quality. Therefore, an appropriately shaped focal spot is essential in many applications, such as optical recording, photolithography and microscopy. Intensive efforts in phase, polarization and amplitude modulation [8–10] of the pupil field have been made to modify the relative ratio between longitudinal and transverse components of the intensity distribution in focus. One simple method is using an annular aperture pupil field to obtain a tighter focusing spot in a high NA system with RP beam illumination, although this happens at the expense of stronger side lobes [11, 12]. It is shown that the longitudinal component of the focused spot can be, depending on the NA, 15% to 30% less than that of the classical Airy spot when shaping the amplitude of the RP pupil field that increases monotonically as a function of the pupil radius [13]. Spot-size reduction by means of focusing such an optimized RP beam with a high NA objective on a photoresist is confirmed experimentally and agrees with the theoretical analysis [14].

Conventional confocal imaging system is a very commonly used microscopic technique, especially in the research field of biology. Due to advantages of laser excitation, high resolution and 2D sections, it is widely applied in biological fluorescent samples. However, the lateral resolution is limited

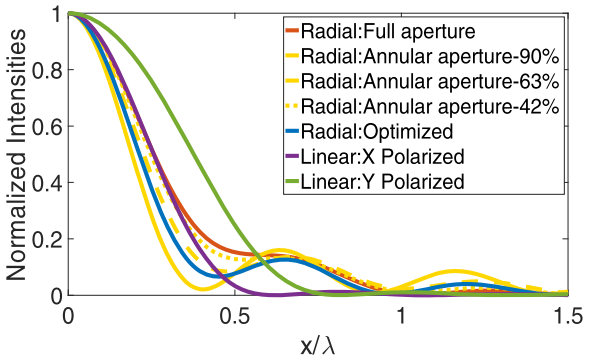

Figure 1. Normalized total intensities of the focal fields for the RP beam with the pupil field of full aperture (red), annular aperture with 90% blocked ring (yellow) in terms of radius, optimized aperture (blue), linearly (purple: along the x axis, green: along the y axis) polarized illumination when the objective NA = 0.9.

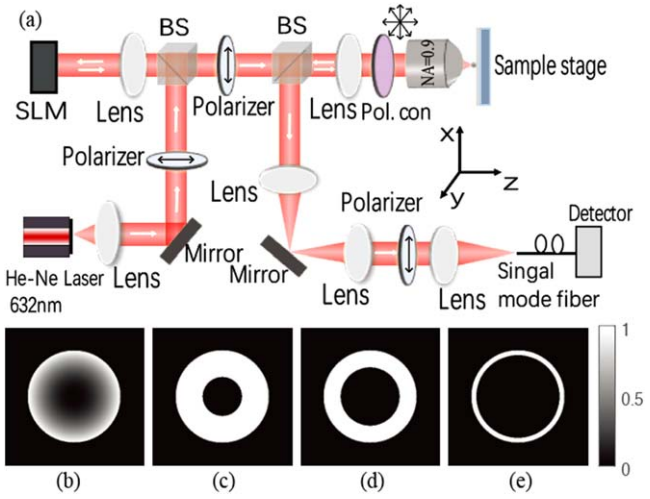

Figure 2. Scheme of the confocal imaging set-up with RP beam excitations (a). SLM modulated amplitude functions: optimized amplitude (b), ring aperture $0.38 < \mathrm{NA} < 0.9$ (c), $0.57 < \mathrm{NA} < 0.9$ (d), and $0.81 < \mathrm{NA} < 0.9$ (e). The grey level represents the amplitude of light (in reflection). Abbreviations: beam splitter (BS), spatial light modulator (SLM), polarization convertor (Pol. con).

by the Abbe diffraction limit. Our motivation for the present research is to implement an amplitude modulated RP beam in a confocal imaging set-up. This will provide general guidance for developing a higher resolution confocal imaging system, which can be not only applied for imaging biological objects but also for nanostructures.

The complete imaging process in a confocal system with a high NA objective illuminated by conventional, annular aperture and amplitude optimized pupil fields of RP beam to obtain a small focused spot is studied theoretically [15]. We first consider the case that the amplitude of the RP beam in the lens pupil is given by

$$g(\rho_p) = \begin{cases} 1 & a - \Delta\rho_p < \rho_p < a \\ 0 & \text{otherwise} \end{cases}, \tag{1}$$

where a is the radius of the pupil of the objective, ρ_p is the radial pupil coordinate, and $\Delta\rho_p$ is the width of the annular ring. The second case is an optimized pupil field which gives the largest longitudinal component of the focused RP beam, for a given power P_0, as derived in [13]:

$$G(k_\perp) = -\frac{k_\perp^{3/2} k^{1/2}}{2\pi i f_1 k_z \Lambda}, \tag{2}$$

and

$$\Lambda = \left(\frac{n\pi}{P_0}\right)^{1/2}\left(\frac{\varepsilon_0}{\mu_0}\right)^{1/2}\frac{1}{\lambda_0}\left(\frac{2}{3} - \sqrt{1-(\mathrm{NA}/n)^2} + \frac{1}{3}\sqrt{(1-(\mathrm{NA}/n)^2)^3}\right)^{1/2}, \tag{3}$$

where the wave vector perpendicular to the optical axis is $\mathbf{k}_\perp = (k_x, k_y)$, with its length $k_\perp = \sqrt{k_x^2 + k_y^2}$ and where $k_z = \sqrt{k^2 - k_\perp^2}$, with $k = k_0 n$ the wave number in the medium with refractive index n, f_1 is the focal distance determined by the objective lens, λ_0 is the wavelength in vacuum, ε_0 and μ_0 are the permittivity and permeability of vacuum, respectively.

Figure 1 shows the advantage of modulating the amplitude of the pupil. Considering the normalized total intensity distribution with NA = 0.9 at focus, the full width at half maximum FWHM $\approx 0.7514\lambda$ of the spot size with linearly y polarized illumination, while FWHM $\approx 0.5186\lambda$ for the case of linearly x polarized illumination. When the illumination is a conventional RP beam, the value of FWHM is the same as the condition of linearly x polarized excitation. However, the optimized pupil function has a FWHM of total intensity 0.434λ, which is 16.3% smaller than the case of conventional RP beam. By blocking 90% in terms of the pupil radius from the center, the value of the FWHM reduces to 0.3916λ, almost 24.5% sharper than the unmodulated conventional RP beam. In our previous simulation work, we regard sub-wavelength particles as electric dipoles, and to make full use of the narrow longitudinal component of the RP beam, two nearby dipoles with longitudinal dipole vectors are considered. It is demonstrated that the smallest distinguished distance of the two ideal longitudinal dipoles is 0.36λ with both annular and optimized pupil fields, i.e. beyond the diffraction limit of 0.68 λ [15]. However, for the annular pupil field, the light only propagates through the 10% unblocked area. As a consequence, the signal is very weak in the experiment. Strong side lobes can be produced in focus, which has a negative influence on imaging a non-isolated object.

The confocal set-up to demonstrate the effect of different focused RP beams is shown in figure 2(a). The He-Ne laser ($\lambda = 632$ nm) passes through a single mode fibre and at the output of the fibre the laser is collimated into a large beam of about 8 mm diameter. The intensity distribution of the laser light is shaped by polarizers and spatial light modulator (SLM), with the latter being a reflected amplitude-only Holoeye LC-R2500.

The first polarizer is to produce linearly polarized light from the unpolarized light and should be aligned with the

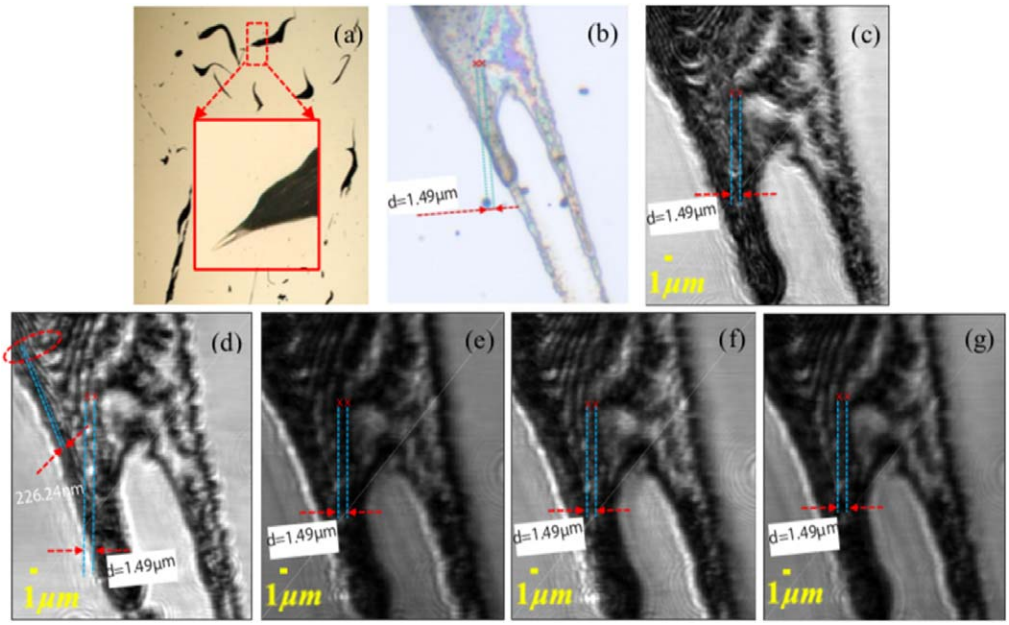

Figure 3. Images of a sample mounted on a substrate resolved by the digital microscope (a) in the wide field view with magnification ×30 and (b) ×2000, and by the improved confocal imaging system with different excitations of RP beams (c) conventional, (d) with optimized amplitude pupil field, and annular pupil fields with (e) 42% blocked, (f) 63% blocked, and (g) 90% blocked.

orientation of liquid crystal molecules in the SLM to maximum the reflectance. The light after modulation passes through the second polarizer between the two beam splitters, which should be cross-polarized for the required amplitude modulation. After that, a liquid-crystal polarization convertor (THORLABS zero-order vortex half-wave retarder) is used to convert the beam from linear to radial polarization by rotating the linear polarization over an angle that depends on the azimuthal angle ϕ in the pupil. The purpose of adding a 4*f* system between the SLM and the objective lens is to avoid the diffraction of modulated light after long distance propagation. Therefore, the modulated pupil field stays the same at the back focal plane as the one produced by the SLM. Then, the RP beam is tightly focused by an objective (NA = 0.9) lens on a sample supported on a substrate. The detected sample is placed on a piezo-electric actuator operating by stepping in the *x*-*y* plane within its linear range. The reflected light goes back to the convertor to convert the light back to linear polarization so that the signal can be easily detected in the confocal system [15, 16]. The final signal is detected after being filtered by the linear polarizer which can improve the image contrast and then collected by a single mode fiber (THORLABS SM600). The fiber with a lens of small NA acts as a pinhole to make an aperture giving 50% of the maximum intensity [17], which is necessary in the confocal microscope. The detector is a silicon photodiode coupled into a low noise amplifier. Figures 2(b)–(e) show the optimum amplitude function given by equations (2) and (3), the annular shaped mask which blocks the center of the beam up to NA = 0.38 (42%), 0.57 (63%) and 0.81 (90%) described in equation (1), respectively. All these modulated pupil fields can be realized by the SLM.

The sample is composed of random structures of paint on a glass substrate ($n_{glass} = 1.5$) with a very thin layer (~20 nm) of TiO2 ($n_{TiO2} = 2.3897$) on top of it. The thin layer functions as a substrate with guided mode excitation to further enhance the resolution and sensitivity [17–20]. A wide view of the sample provided by the digital microscope KEYENCE VHX-6000 is shown in figure 3(a) with the magnification ×30. The area in the red dashed box amplified as an inset is the final research target, which is zoomed in by 2000 times in figure 3(b). Here, we need to draw attention to the magnification defined by Keyence microscope, which is very high and thus different from the normal optical magnification. In fact, there is a multiplication factor of ~22 after the calibration. One group of strips which can be distinguished are separated by $d = 1.49\ \mu$m. Figures 3(c)–(g) display the images of the area obtained by our confocal imaging system with the excitations of a scanning focused spot corresponding to the conventional RP beam (c), to the optimized RP beam (d) and the annular mask with 42% (e), 63% (f) and 90% (g) of the light being blocked. The stripes with various distances in the structure are useful to determine the spatial resolution. The marked stripes with a distance of $d = 1.49\ \mu$m in figure 3(b) can be seen in all the images obtained with the amplitude modulated RP beams (figures 3(d)–(g)), except in the case of the conventional RP beam (figure 3(c)). In figure 3(d), after the sample illuminated by the RP beam with the optimized pupil field as described in equations (2) and (3), even the distance of 226.24 nm(0.358λ) between two stripes can be observed clearly. The highly resolved distance agrees well with the resolution of $d = 0.36\lambda$ as mentioned in our previous theoretical calculation [15]. For the annular pupil fields, the medium size of the ring aperture (63% blocked) gives the best imaging result. This is reasonable, since with the increase of the blocked area (figure 3(g)), the effect of the side lobes becomes significant. Therefore, in the experiment, the image quality is not so good with the illumination of the RP beam of the annular aperture (90% blocked) as predicted in the simulations. Another important

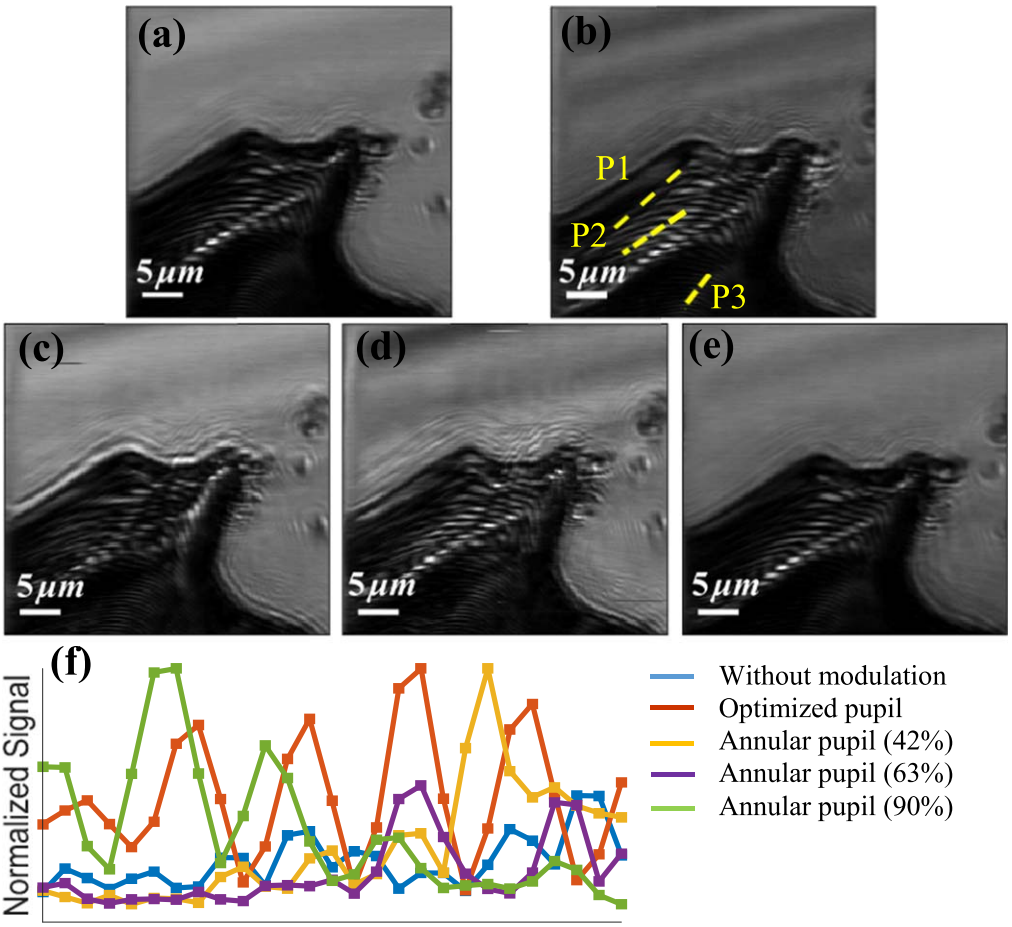

Figure 4. Images of another scanning area of the sample mounted on a substrate resolved by the improved confocal imaging system with different excitations of RP beams (a) conventional, (b) with optimized amplitude pupil field, and annular pupil fields with (c) 42% blocked, (d) 63% blocked, and (e) 90% blocked. Cross sections are shown in (f) to make comparisons of the visibility in above five cases.

reason is that the sample is not the ideal longitudinal dipole anymore in the experimental work. Although the image quality in figure 3(e) with 42% of the pupil light being blocked is worse than the other two annular aperture cases (figures 3(f) and (g)), it is better than the unmodulated conventional condition (figure 3(c)). Therefore, the RP beam with the optimized amplitude of pupil field gives the most amount of detailed information and the best resolution. The RP beam with the pupil field of an annular ring also has advantages in the application of imaging, but the size of the ring mask should be chosen properly.

Figure 4 shows another larger scanning area (40 μm × 40 μm) of the sample with five different RP beam illuminations. The scanning is with a step size of 0.20 μm. It is not difficult to see that the optimized and annular RP beam excitation in figures 4(b) and (d) give the best resolutions among the five conditions (figures 4(a)–(e)), especially at the center part of the black-white stripes. In order to quantify the quality of the image, we use the visibility defined by:

$$visibility = \frac{I_{\max} - I_{\min}}{I_{\max} + I_{\min}}, \tag{4}$$

with $I_{\max}$ and $I_{\min}$ the maximum and minimum normalized intensities. The higher the visibility is, the better image quality is achieved. Figure 4(f) presents the normalized signal distributions at the position of yellow dashed line labeled P1 as shown in figure 4(b), and also at the same position for other four conditions. The main reason to choose this position is that, in figures 4(b) and (d), the stripes can be found, but in the other three images, these stripes cannot be observed clearly. Thus, this position is interesting and worth analyzing with visibility. The fluctuations in figure 4(f) are related to the dark and bright stripes in the subplots. It can be found that there are some position shifts of the peaks and valleys in five conditions due to the scanning of the sample. It is difficult to keep going back to the same original position with the sample. Thus, we compute the average visibility in the certain range shown in figure 4(f) and they are 0.2599 (blue), 0.7196 (red), 0.3127 (yellow), 0.5731 (purple) and 0.5312 (green), respectively. The two lines labeled P2 and P3 as shown in figure 4(b) are also investigated. The corresponding average visibilities are listed in table 1. The method to quantify the resolution is to differentiate the measured intensity with

Table 1. Average visibilities for different modulated RP beams.

Position	Unmodulated	Optimized	42%	63%	90%
1	0.2599	**0.7196**	0.3127	**0.5731**	0.5312
2	0.2175	**0.5959**	0.3149	**0.4775**	0.3701
3	0.0116	**0.0908**	0.0237	**0.0562**	0.0228

respect to position and the definition of the derivation is defined as follows:

$$derivation = \sqrt{\left(\frac{\partial I}{\partial x}\right)^2 + \left(\frac{\partial I}{\partial y}\right)^2}, \quad (5)$$

where I is the normalized intensity at each position. The case with highest derivative has the highest resolution. Through calculating the derivation along the dashed line P2 in five conditions. The average value is 0.0384 (without modulation), 0.0689 (optimized pupil), 0.0455 (annular pupil 42% blocked), 0.0573 (annular pupil 63% blocked) and 0.0462 (annular pupil 92% blocked). From the data, it is clear that the optimized RP pupil field can provide best image resolution and quality, which is much better than the unmodulated conventional RP pupil field. Annular RP pupil fields can improve the image quality compared to the conventional RP beam illumination to some extent. It is shown that with the medium sized ring, the quality of the image is the best. Thus, the size of the ring mask should be chosen properly before making use of it, as the effect of side lobes and the strength of the signal should be taken into account. This result is consistent with images presented in figure 3.

In conclusion, we show the effect of amplitude modulated RP beams in the resolution of a confocal imaging system. Our previous theoretical prediction is confirmed [15]. With SLM, we have been able to obtain the optimized pupil field and annular aperture pupil fields with different ring sizes, and shown that the performance of the confocal imaging system is improved, resulting in better image quality than that provided by the conventional RP beam. The smallest distinguishable distance of two nearby strips is $d = 0.358\lambda$ in the experiment with the optimized RP beam, which is beyond the diffraction limit. Such results match very well with the simulated value $d = 0.36\lambda$. Instead of considering the usual fluorescent samples, our experimental results apply to non-fluorescent samples. We believe that by combining the superiority of the amplitude modulated RP beam with the confocal imaging system should open up an avenue for applying high resolved imaging technique in not only biological and medical research fields, but also other fields, such as nanostructure characterization.

Acknowledgments

We acknowledge the Project 17FUN01 'BeCOMe' within the programme EMPIR. The EMPIR initiative is co-founded by the Europeam Union's Horizon 2020 research and innovation programme and the EMPIR Participating Countries. We acknowledge the funding from China Scholarship Council and Erasmus. We also thank Thomas Siefke from Friedrich Schiller University, Jena for the fabrication of the nanolayer on the glass substrate.

ORCID iDs

Peiwen Meng https://orcid.org/0000-0003-2888-5675

References

[1] Quabis S, Dorn R, Eberler M, Glöckl O and Leuchs G 2000 *Opt. Commun.* **179** 1
[2] Youngworth K S and Brown T G 2000 *Opt. Express* **7** 77
[3] Zhan Q 2004 *Opt. Express* **12** 3377
[4] Dholakia K and Čižmár T 2011 *Nat. Photonics* **5** 355
[5] Zhang Y and Bai J 2009 *Opt. Express* **17** 3698
[6] Varin C *et al* 2013 *Applied Sciences* **3** 70
[7] Kozawa Y, Matsunaga D and Sato S 2018 *Optica.* **5** 86
[8] Dorn R, Quabis S and Leuchs G 2003 *Phys. Rev. Lett.* **91** 233901
[9] Wang H, Shi L, Lukyanchuk B, Sheppard C and Chong C T 2008 *Nat. Photonics* **2** 501
[10] Khonina S N, Karpeev S V, Alferov S V and Soifer V A 2015 *J. Opt.* **17** 065001
[11] Sheppard C J R and Choudhury A 2004 *Appl. Opt.* **43** 4322
[12] Yang L, Xie X, Wang S and Zhou J 2013 *Opt. Lett.* **38** 1331
[13] Urbach H P and Pereira S F 2008 *Phys. Rev. Lett.* **100** 123904
[14] Ushakova K, Van de Berg Q, Pereira S F and Urbach H P 2015 *J. Opt.* **17** 125615
[15] Meng P, Pereira S F and Urbach H P 2018 *Opt. Express* **26** 29600
[16] Xie X, Chen Y, Yang K and Zhou J 2014 *Phys. Rev. Lett.* **113** 263901
[17] Murphy D B 2002 *Fundamentals of Light Microscopy and Electronic Imaging* (New York: Wiley)
[18] Roy S, Pereira S F, Urbach H P, Wei X and Gawhary O E 2017 *Phys. Rev.* A **96** 013814
[19] Gawhary O E, Dheur M, Pereira S F and Braat J J M 2013 *Appl. Phys.* B **111** 637
[20] Roy S, Ushakova K, Berg Q, Pereira S F and Urbach H P 2015 *Phys. Rev. Lett.* **114** 103903